Geochemistry Geophysics Geosystems G3
AN ELECTRONIC JOURNAL OF THE EARTH SCIENCES
Published by AGU and the Geochemical Society

Article
Volume 9, Number 7
9 July 2008
Q07008, doi:10.1029/2008GC002081
ISSN: 1525-2027

Estimating pore-space gas hydrate saturations from well log acoustic data

Myung W. Lee
U.S. Geological Survey, Box 25046, MS-939, Denver Federal Center, Denver, Colorado 80225, USA (mlee@usgs.gov)

William F. Waite
U.S. Geological Survey, 384 Woods Hole Road, Woods Hole, Massachusetts 02543, USA

[1] Relating pore-space gas hydrate saturation to sonic velocity data is important for remotely estimating gas hydrate concentration in sediment. In the present study, sonic velocities of gas hydrate–bearing sands are modeled using a three-phase Biot-type theory in which sand, gas hydrate, and pore fluid form three homogeneous, interwoven frameworks. This theory is developed using well log compressional and shear wave velocity data from the Mallik 5L-38 permafrost gas hydrate research well in Canada and applied to well log data from hydrate-bearing sands in the Alaskan permafrost, Gulf of Mexico, and northern Cascadia margin. Velocity-based gas hydrate saturation estimates are in good agreement with Nuclear Magneto Resonance and resistivity log estimates over the complete range of observed gas hydrate saturations.

Components: 4395 words, 5 figures, 1 table.

Keywords: methane hydrate; seismic velocity; hydrate assessment.

Index Terms: 3004 Marine Geology and Geophysics: Gas and hydrate systems; 3025 Marine Geology and Geophysics: Marine seismics (0935, 7294); 0702 Cryosphere: Permafrost (0475).

Received 30 April 2008; **Revised** 27 May 2008; **Accepted** 3 June 2008; **Published** 9 July 2008.

Lee, M. W., and W. F. Waite (2008), Estimating pore-space gas hydrate saturations from well log acoustic data, *Geochem. Geophys. Geosyst.*, *9*, Q07008, doi:10.1029/2008GC002081.

1. Introduction

[2] Gas hydrates are ice-like crystalline solids in which small-diameter guest molecules occupy and stabilize cages composed of water molecules. Methane is the most common naturally occurring guest molecule, and methane hydrates are distributed worldwide in continental margin sediments and beneath permafrost where relatively high pressures and low temperatures stabilize the hydrate structure [*Kvenvolden and Lorenson*, 2001].

[3] Hydrate-rich sand layers represent potential targets for extracting methane as an energy resource, but remote-sensing techniques are required to assess the hydrate content and resource potential. In sands, gas hydrate growth tends to displace pore fluids. Because gas hydrates exhibit relatively high compressional (P wave) and shear (S wave) velocities compared to those of pore-filling fluids, the presence of gas hydrate tends to elevate measured wave velocities through gas hydrate–bearing sediment (GHBS) [*Stoll and Bryan*, 1979]. Using seismic techniques to detect and quantify the gas hydrate volume in sediment requires a predictive

model relating the pore-space gas hydrate content to measured elastic velocities.

[4] Many velocity model forms have been applied to GHBS, including (1) time-average equations [*Wood et al.*, 1994]; (2) weighted equations [*Lee and Collett*, 1999]; (3) cementation theory [*Ecker et al.*, 1998; *Guerin et al.*, 1999]; (4) effective medium theory [*Helgerud et al.*, 1999; *Jakobsen et al.*, 2000]; (5) modified Biot-Gassmann theory [*Lee and Collett*, 2005]; and (6) three-phase Biot-type equations [*Carcione and Gei*, 2004; *Carcione and Tinivella*, 2000].

[5] Recent studies favor load-bearing models for naturally occurring gas hydrate, whereby hydrate grows in pores, partially supporting the sediment frame [*Kleinberg et al.*, 2005]. We present one such model: a new three-phase, Biot-type relation between sonic wave velocities in unconsolidated sands and the pore-space hydrate saturation. This model is developed using well log measurements from the Mallik 5L-38 Canadian permafrost gas hydrate research well, then applied to measurements from the Mt. Elbert Alaskan permafrost gas hydrate research well, the Tigershark marine gas hydrate research well in the Gulf of Mexico, and the International Ocean Drilling Program (IOPD) Expedition 311 Site U1326D well in the northern Cascadia margin offshore Vancouver Island.

2. Theory

2.1. Derivation of the Three-Phase Equation

[6] On the basis of the work of *Leclaire et al.* [1994], *Carcione and Tinivella* [2000] developed a three-phase Biot-type equation (TPBE) to compute elastic velocities through GHBS. This approach assumes an idealized arrangement in which sediment, hydrate and pore fluid form three homogeneous, interwoven frameworks. Each framework has characteristic bulk and shear moduli, which contribute to the overall P and S wave speed through the matrix elements R_{ij} and μ_{ij} presented below. These elements are discussed further by *Carcione and Tinivella* [2000, Appendix A]. Following the method of *Leclaire et al.* [1994], TPBE calculates the eigenvalues of the R_{ij} and μ_{ij} matrices, and predicts a fast P wave with velocity V_p, two slow P waves, a fast S wave with velocity V_s, and one slow S wave. Because dispersion of the fast waves is negligible below the logging frequency of ~30 kHz, we neglect attenuation and assume the elements of R_{ij} and μ_{ij} are real. With these assumptions, fast velocities of gas hydrate–bearing sediments at low frequencies can be calculated from [*Lee*, 2007]:

$$V_p = \sqrt{\frac{\sum_{i,j=1}^{3} R_{ij}}{\rho_b}} \text{ and } V_s = \sqrt{\frac{\sum_{i,j=1}^{3} \mu_{ij}}{\rho_b}} \tag{1}$$

where the GHBS bulk density, ρ_b, is given by $\rho_b = (1-\phi)\rho_s + (1-C_h)\phi\rho_w + C_h\phi\rho_h$, ϕ is porosity, C_h is the pore space hydrate saturation, and subscripts s, w, and h refer to sediment grain, water, and hydrate, respectively. For low frequencies in the absence of hydrate, equation (1) reduces to the formation moduli given by *Gassmann* [1951].

[7] The elements of R_{ij} and μ_{ij} are given by:

$$\begin{gathered}
R_{11} = [(1-c_1)\phi_s]^2 K_{av} + K_{sm} + 4\mu_{11}/3 \\
R_{12} = R_{21} = (1-c_1)\phi_s\phi_w K_{av} \\
R_{13} = R_{31} = (1-c_1)(1-c_3)\phi_s\phi_h K_{av} + 2\mu_{13}/3 \\
R_{22} = \phi_w^2 K_{av} \\
R_{23} = (1-c_3)\phi_h\phi_w K_{av} \\
R_{33} = [(1-c_3)\phi_h]^2 K_{av} + K_{hm} + 4\mu_{33}/3 \\
\mu_{11} = [(1-g_1)\phi_s]^2 \mu_{av} + \mu_{sm} \\
\mu_{12} = \mu_{21} = \mu_{22} = \mu_{23} = \mu_{32} = 0 \\
\mu_{13} = (1-g_1)(1-g_3)\phi_s\phi_h\mu_{av} + \mu_{sh} \\
\mu_{33} = [(1-g_3)\phi_h]^2 \mu_{av} + \mu_{hm}
\end{gathered} \tag{2}$$

where

$$\begin{gathered}
\phi_s = 1-\phi, \phi_w = (1-C_h)\phi, \phi_h = C_h\phi, \\
c_1 = \frac{K_{sm}}{\phi_s K_s}, \; c_3 = \frac{K_{hm}}{\phi_h K_h}, \; g_1 = \frac{\mu_{sm}}{\phi_s \mu_s}, \; g_3 = \frac{\mu_{hm}}{\phi_h \mu_h}, \\
K_{av} = \left[\frac{(1-c_1)\phi_s}{K_s} + \frac{\phi_w}{K_w} + \frac{(1-c_3)\phi_h}{K_h}\right]^{-1}, \\
\mu_{av} = \left[\frac{(1-g_1)\phi_s}{\mu_s} + \frac{\phi_w}{2\omega\eta} + \frac{(1-g_3)\phi_h}{\mu_h}\right]^{-1},
\end{gathered}$$

ω is an angular frequency, K is the bulk modulus, μ is the shear modulus, and η is the pore fluid viscosity. The subscripts *sm* and *hm* refer to the sediment framework and hydrate framework, respectively. Framework moduli are given below.

[8] Key elements for deriving velocities from equation (1) are R_{11}, R_{33}, μ_{11} and μ_{33}. To compute these elements, bulk and shear moduli for the frameworks formed by each phase in the three-phase system must be obtained. The pore fluid framework stiffness depends only on the volume fraction, ϕ_w, and moduli, K_w, and $\omega\eta$, of the pore fluid. *Carcione and Tinivella* [2000] derived the sediment and hydrate framework moduli using the Kuster-Toksöz theory [*Kuster and Toksöz*, 1974].

Here, however, we derive bulk and shear moduli for both the sediment and hydrate frameworks from the expressions proposed by *Pride et al.* [2004] and *Lee* [2005] for a dry framework:

$$K_d = \frac{K_s(1-\phi)}{(1+\alpha\phi)}, \tag{3}$$

$$\mu_d = \frac{\mu_s(1-\phi)}{(1+\gamma\alpha\phi)}, \tag{4}$$

with

$$\gamma = \frac{1+2\alpha}{1+\alpha}, \tag{5}$$

where K_d and μ_d are the bulk and shear moduli of the dry framework, and K_s and μ_s are the bulk and shear moduli of the grains making up that framework. As shown below, we replace the grain moduli, K_s and μ_s, and the porosity ϕ, with the moduli and porosity appropriate for the hydrate framework (section 2.2), or the sediment framework (section 2.3), to obtain the framework moduli K_{hm}, μ_{hm}, K_{sm}, and μ_{sm} required in equation (2).

[9] The consolidation parameter, α, accounts for sediment stiffening due to consolidation, which increases the sediment moduli by reducing the porosity and increasing intergranular contacts. As described by *Lee* [2005], α is estimated by using equations (3) and (4) in equation (1) to fit P wave speed measurements, and S wave speed measurements if they are available, in hydrate-free zones neighboring hydrate-bearing sands. Once the local degree of consolidation, as estimated by α, is known, equations (3) and (4) are used to predict bulk and shear moduli in the hydrate-bearing sand targets. As α increases, dry frame moduli decrease, decreasing the velocity. If $\gamma = 1.5$, equation (4) is identical to that recommended by *Pride et al.* [2004].

2.2. Gas Hydrate Framework Moduli

[10] Porosity, ϕ, in equations (3) and (4) denotes the non-framework volume fraction. For the gas hydrate framework, the non-hydrate volume fraction is:

$$\phi_{ah} = 1 - \phi_h, \tag{6}$$

so the bulk, K_{hm}, and shear, μ_{hm}, moduli of the hydrate become:

$$K_{hm} = \frac{K_h(1-\phi_{ah})}{(1+\alpha\phi_{ah})} \text{ and } \mu_{hm} = \frac{\mu_h(1-\phi_{ah})}{(1+\gamma\alpha\phi_{ah})}. \tag{7}$$

2.3. Sediment Framework Moduli

[11] If the sediment framework undergoes compaction, the moduli increase as ϕ decreases according to equations (3) and (4). Hydrate formation decreases the water-filled porosity from ϕ to ϕ_w, and if that were equivalent to compaction, the sediment framework moduli could be calculated from equations (3) and (4) by substituting ϕ_w for ϕ. The resulting moduli lead to velocity estimates in equation (1) that exceed the measured values, however. We instead use an apparent porosity for the sediment framework, ϕ_{as}, given by:

$$\phi_{as} = \phi_w + \varepsilon\phi_h, \tag{8}$$

where the parameter ε accounts for the reduced impact of hydrate formation relative to compaction in terms of stiffening the host sediment framework. Using the apparent porosity ϕ_{as}, the sediment framework moduli, K_{sm} and μ_{sm}, become:

$$K_{sm} = \frac{K_s(1-\phi_{as})}{(1+\alpha\phi_{as})} \text{ and } \mu_{sm} = \frac{\mu_s(1-\phi_{as})}{(1+\gamma\alpha\phi_{as})}. \tag{9}$$

[12] If $\varepsilon = 1$, hydrate floats in the pore space, does not contact sediment grains or support any of the sediment load. This is the smallest effect gas hydrate formation can have on sediment stiffness. If $\varepsilon = 0$, equation (8) reduces to $\phi_{as} = \phi_w$. This implies hydrate is treated like a sediment grain, replacing pore fluid and forming efficient load-supporting contacts between sediment grains in a manner equivalent to the effect of compaction in terms of sediment stiffening. We initially determined ε empirically, but as shown below, ε does not appear to vary from site to site and can be considered constant.

3. Application

3.1. Modeling Mallik 5L-38 Acoustic Velocity Data

[13] Figure 1 compares a subset of the Mallik 5L-38 well log data with P and S wave velocities from TPBE as well as from an effective medium model (EMT) [*Helgerud et al.*, 1999] and the modified Biot-Gassmann theory (BGTL) [*Lee and Collett*,

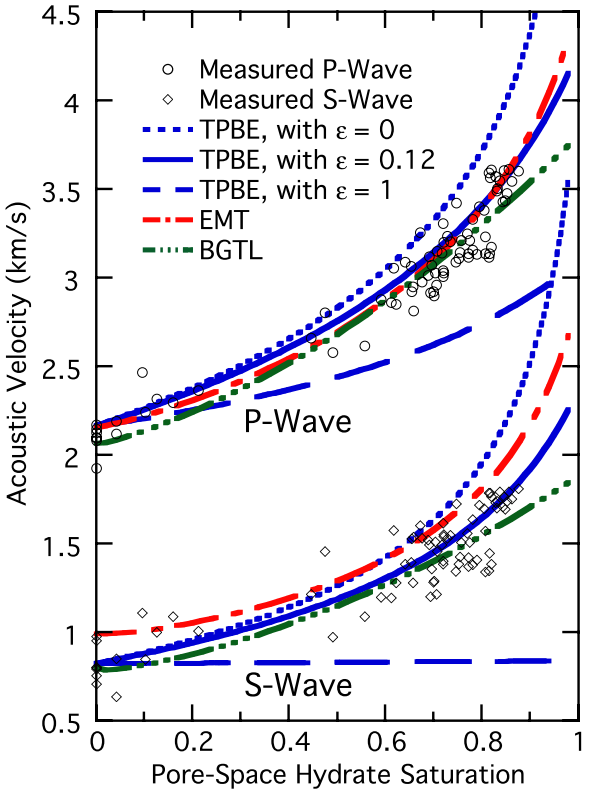

Figure 1. Modeled and measured P and S wave velocities at the Mallik 5L-38 permafrost gas hydrate research well, western Canada. Measured velocities are the subset of gas hydrate–bearing sediments with porosity between 34 and 35% and clay content less than 20%. Velocities are modeled using the three-phase Biot-type equation (TPBE), with $\alpha = 25$ and $\varepsilon = 0$, 0.12, and 1; effective medium theory (EMT) with critical porosity of 0.4 and effective pressure of 5 MPa; and the modified Biot-Gassmann theory (BGTL) with $n = 1.14$. Common parameters are the sediment porosity of 0.345, fractional clay volume of 0.1.

1999]. Both EMT and BGTL describe hydrate as "pore filling," but like TPBE, utilize mathematical formulations describing load-bearing hydrate distributions. *Helgerud et al.* [1999] and *Lee and Collett* [1999] used "pore filling" to differentiate their models from cementation models, rather than to describe pore-filling hydrate that does not support the sediment frame.

[14] TPBE is intended to model hydrate occurrences in sands, rather than clay-rich sediment. This restriction is due to the assumption in Biot theory that pore water is not bound to the sediment grains. As the clay content increases, the percentage of pore water bound to the clay particles increases, and the pore water assumptions underlying TPBE and other Biot-based models begin to break down. Therefore, measured data for the Mallik 5L-38 well were taken from the hydrate-bearing intervals between 891 and 1,109 m, and included only measurements through sediment with 34–35% porosity and clay content, C_v, less than 0.2. The models assume $\phi = 34.5\%$, $C_v = 0.1$, and an effective pressure of 5 MPa. Elastic parameters for the sediment constituents are given in Table 1. Baseline P and S wave velocities through hydrate-free sediment, using TPBE with $\alpha = 25$, are 2.21 km/s and 0.78 km/s, respectively. As the gas hydrate saturation increases, both P and S wave velocities increase, reaching 3.7 km/s and 1.9 km/s at 90% saturation, respectively. The V_P/V_S ratio decreases with increasing gas hydrate content, falling below 2.0 for gas hydrate saturations above ~70%.

[15] For each model, free parameters were chosen to optimize the P wave speed fit. Differences in predictive capabilities between models are therefore highlighted by differences in the S wave speed fits obtained using those same free parameters. For the EMT [*Helgerud et al.*, 1999], P wave velocities modeled assuming a critical porosity $\phi_c = 40\%$, and effective pressure $P = 5$ MPa, are virtually identical to the TPBE predictions below ~70% gas hydrate saturation. EMT-predicted S wave velocities exceed the measured results for all saturations, however.

[16] Velocities modeled using BGTL [*Lee and Collett*, 2005], with an assumed S wave velocity exponent parameter $n = 1.14$, are similar to those from the TPBE for hydrate saturations up to about 75%, but are smaller for higher saturations. TPBE better matches the more rapid S wave velocity increase as hydrate saturation increases above 75%.

3.2. Estimating Pore-Space Gas Hydrate Saturations at Mallik 5L-38

[17] Figure 2 shows gas hydrate saturations estimated from the NMR log, the P wave velocity, and

Table 1. Elastic Parameters for the Sediment Constituents[a]

Material	ρ (g/cc)	K (GPa)	G (GPa)
Quartz	2.65	36.6	45.0
Methane hydrate	0.91	6.41	2.54
Clay	2.58	20.9	6.85
Water	1	2.25	0

[a] Quartz and clay data from *Helgerud et al.* [1999]. Water data from *Mavko et al.* [1998]. Methane hydrate moduli calculated from the P and S wave velocities and density from *Sloan* [1998].

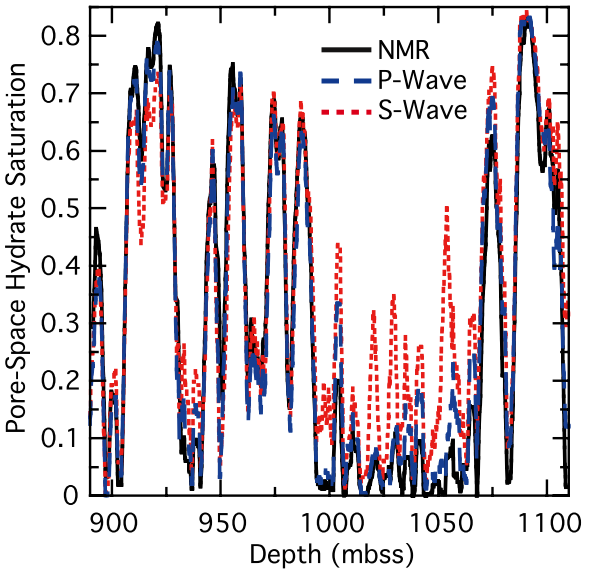

Figure 2. Gas hydrate saturation estimated from NMR and acoustic logs at the Mallik 5L-38 well, western Canada. Depth is given in meters below the sediment surface (mbss). All saturations are smoothed using a 21-point (3-m) running average.

the S wave velocity at the Mallik 5L-38 well for depths between 891 and 1109 m using a depth-dependent α obtained from velocity fits in non-reservoir intervals. Our saturation predictions use the measured porosity and clay content estimated from the gamma log rather than assuming these parameters are constant, and the saturation estimates are comparable to those from the resistivity log [*Kleinberg et al.*, 2005]. The P wave prediction of hydrate saturation differs from the NMR estimate by, on average, 0.04 over the entire depth interval between 891 and 1110 m depth. The S wave prediction differs by an average of 0.08 from the NMR estimate over the same interval, but only by an average of 0.06 in the hydrate-rich intervals spanning 890 to 1000 m and 1070 to 1110 m depth.

4. Discussion

[18] There are two free parameters, α and ε, to be determined when using TPBE to fit measured velocities. The consolidation parameter, α, primarily depends on porosity and effective pressure, and is determined by fitting TPBE velocity predictions to P and S wave velocities in hydrate-free sediment adjacent to the target GHBS [*Lee*, 2005]. Having been determined on the basis of velocities in hydrate-free sediment, α is not varied to optimize the velocity fit for the target GHBS. If the hydrate-free sediment data is robust enough to provide a depth-dependent α, as is the case for Mallik 5L-38 (Figure 2), this can improve the hydrate saturation estimate. A constant α is sufficient in most locations, as demonstrated below. In sites where hydrate-free data are difficult to obtain, or the extent of compaction is rapidly changing with depth, α may be poorly constrained. As shown in section 4.4, however, even 20% errors in α lead to errors of only 0.1 or less in the predicted hydrate saturation.

[19] Hydrate growth reduces the sediment porosity. The parameter ε captures the effectiveness of this porosity reduction in increasing the sediment moduli and hence, controls how fast velocity increases with increasing gas hydrate saturation (Figure 1). The value $\varepsilon = 0.12$ optimizes the velocity fit to the Mallik 5L-38 data. This value indicates hydrate does not merely float in the pore space without contacting sediment grains ($\varepsilon = 1$), but instead supports a portion of the sediment load and stiffens the host sediment framework. The resulting moduli increase can be significant, but not as great as would be expected for compaction, where porosity is replaced by host sediment grain material ($\varepsilon = 0$). Since $\varepsilon = 0$ yields the largest sediment stiffness increase hydrate can impart without cementing the grains, the use of $\varepsilon = 0.12$ here suggests hydrate does not act as a cement.

[20] Below, we examine the effectiveness of TPBE in permafrost and marine GHBS over a range of porosities and subbottom depths. Though the geological environment, porosity, and effective pressure vary widely from site to site, the Mallik 5L-38 well and the three examples below highlight two important aspects of the parameters α and ε: (1) α generally decreases with increasing subbottom depth, implying as expected that consolidation leads to increased stiffness with increasing depth. (2) Setting $\varepsilon = 0.12$ provides reasonable fits in both permafrost and marine hydrate-bearing sands as demonstrated below, suggesting ε can be considered constant, rather than being a site-specific free parameter.

4.1. Permafrost GHBS, Milne Point, Alaska

[21] Setting $\varepsilon = 0.12$ with $\alpha = 34$ produces reasonable fits for velocity data through hydrate-bearing sand layers at the Mt. Elbert permafrost gas hydrate research well at Milne Point, Alaska (Figure 3) [*Mount Elbert Science Team*, 2007]. The Mt. Elbert GHBS has porosities ranging from 25% to 45%, and an effective pressure of ~7 MPa, and

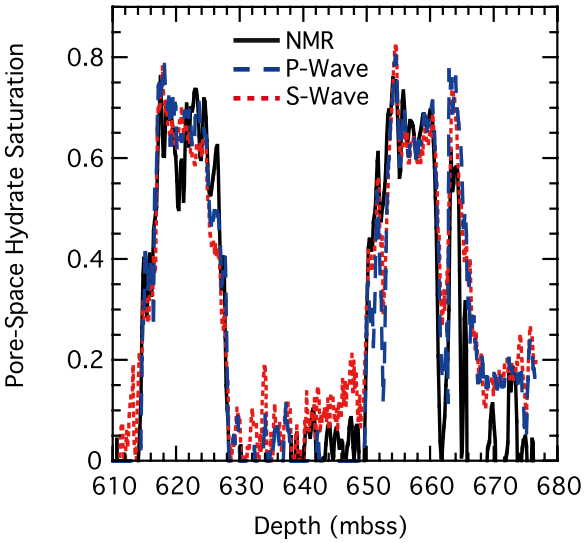

Figure 3. Gas hydrate saturations estimated from NMR and P and S wave acoustic logs at the Mount Elbert gas hydrate research well at Milne Point, Alaskan North Slope. Depth is given in meters below the sediment surface (mbss).

the gas hydrate saturations estimated from the P wave velocities are almost identical to those estimated from the S wave velocities.

4.2. Marine GHBS, Tigershark Well, Gulf of Mexico

[22] Setting $\varepsilon = 0.12$ with $\alpha = 35$ works well for hydrate-bearing sands at the Tigershark well in Alaminos Canyon lease block 818 in the Gulf of Mexico (Figure 4), where porosities ranged from 40% to 48%, with an effective pressure of ~4 MPa [*Smith et al.*, 2006]. Because the resistivity logging tool has a lower vertical resolution than the acoustic logging tool does, the gas hydrate–bearing sediments estimated from the resistivity log appear thicker than in the acoustic predictions.

4.3. Marine GHBS, IODP Hole U1326, Cascadia Margin

[23] Data from IODP Site U1326, drilled during Expedition 311 in the Cascadia margin offshore Vancouver Island [*Expedition 311 Scientists*, 2006] provide an example of estimating gas hydrate saturations in high-porosity, shallow sediment for which the effective pressure is only ~0.5 to 2 MPa. Figure 5 compares saturations estimated from the resistivity log with those estimated from the P wave velocities at IODP Hole U1326D. We estimate $\alpha = 40$ from the P wave velocity fit near 150 m below seafloor (mbsf), and again hold $\varepsilon = 0.12$. S wave velocities are also measured in this well, but we did not include them in our study because of their poor quality. Because porosity was not measured at this well, we used the porosity measured at a nearby well, U1326A, located about 20 m from the U1326D [*Expedition 311 Scientists*, 2006]. Porosities ranged from 30% to 60% at this well, with porosities of 40% for the high gas hydrate saturations near 50 m subbottom depth, and porosities of 55% for the moderate gas hydrate saturation depths near 225 m below seafloor.

4.4. Fit Parameter Sensitivity

[24] Errors in choosing the fit parameters α and ε impact the predicted hydrate saturation, but as shown below, even moderate fit parameter errors change the predicted hydrate saturation by only 0.1 or less.

[25] The fit parameter sensitivity is most pronounced for S wave estimates of hydrate saturation. The fractional S wave velocity change ($\Delta V_s/V_s$) associated with a fractional change in the consolidation parameter ($\Delta\alpha/\alpha$) is given by:

$$\frac{\Delta V_S}{V_s} = \frac{-\alpha\gamma\phi}{2(1+\gamma\alpha\phi)}\frac{\Delta\alpha}{\alpha}. \tag{10}$$

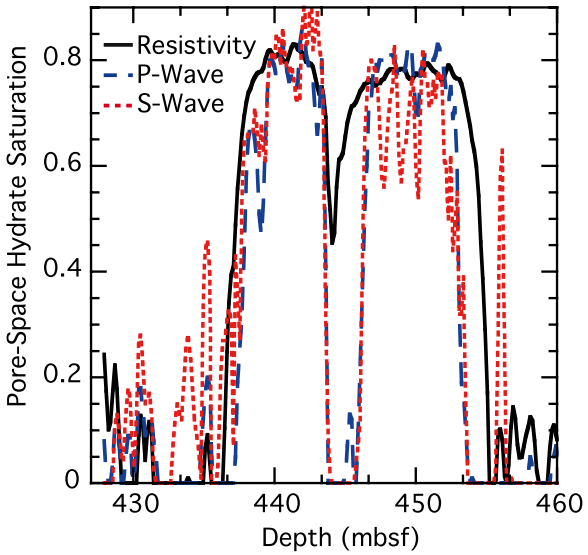

Figure 4. Gas hydrate saturation estimated from electrical resistivity and P wave and S wave acoustic logs at the Tigershark well, Gulf of Mexico. Depth is given in meters below the seafloor (mbsf). The apparent thicker gas hydrate–bearing sediments estimated from the resistivity log are primarily caused by a difference of vertical resolution capabilities of the logging tools.

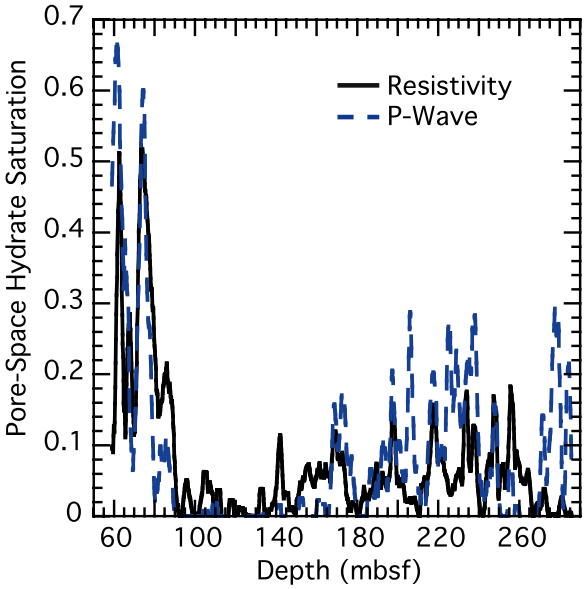

Figure 5. Gas hydrate saturation estimated from resistivity and P wave acoustic logs at the U1326D well, IODP Expedition 311, Cascadia margin, offshore Vancouver Island. Depth is given in meters below the seafloor (mbsf). All saturations are smoothed using a 15-point (2.3-m) running average.

[26] For typical values of unconsolidated sediments with $\phi = 0.4$ and $\alpha = 30$, the fractional change of the S wave velocity is about 10% when $\Delta\alpha/\alpha = 0.2$. In other words, a 20% increase in α reduces the S wave velocity by about 10%.

[27] The error in the hydrate saturation prediction, ΔC_h, depends on the S wave velocity error according to:

$$\Delta C_h \approx \frac{2(1-\phi_{as})(1+\gamma\alpha\phi_{as})}{\phi(1-\varepsilon)(1+\alpha\gamma)}\frac{\Delta V_s}{V_s}, \qquad (11)$$

which indicates the hydrate saturation prediction becomes less sensitive to velocity errors as the porosity increases, or as V_s increases owing to an increasing hydrate saturation. For $\phi = 0.4$ and $C_h = 0.6$, the 10% error in V_s discussed above changes the hydrate saturation prediction by 0.1. The sensitivity is smaller when hydrate saturations are estimated from P wave speeds.

[28] The parameter ε affects the hydrate saturation prediction through the apparent porosity, with a sensitivity given by:

$$\Delta C_h = \frac{C_h}{(1-\varepsilon)}\Delta\varepsilon. \qquad (12)$$

We used $\varepsilon = 0.12$ for all sites considered here. Even for $\Delta\varepsilon = 0.05$, ΔC_h is less than 0.06 for the fully hydrate-saturated system, $C_h = 1$, and diminishes as the hydrate saturation decreases. As long as ε is close to 0.12, C_h is not sensitive to the exact choice of ε.

5. Conclusions

[29] The three-phase Biot-type equation, TPBE, models the effect of gas hydrate on sonic velocity by treating gas hydrate as a homogeneous, load-bearing sediment component. TPBE introduces two fitting parameters, α and ε. The parameter α captures the extent of sediment consolidation and is determined locally from the P and/or S wave speeds in hydrate-free sediment adjacent to the target GHBS.

[30] Hydrate formation reduces the sediment porosity, and the parameter ε captures the effectiveness of that porosity reduction in stiffening the sediment. In both marine and permafrost settings over a variety of porosities and subbottom depths, $\varepsilon = 0.12$ provides a reasonable prediction of gas hydrate saturation, suggesting the parameter can be considered a constant, with negligible site-to-site variability. The value of 0.12 suggests, for all locations considered here, that gas hydrate does not merely float in the pore space ($\varepsilon = 1$), but instead contacts sediment grains and acts as a load-bearing, non-cementing sediment component. Though hydrate formation stiffens the sediment, the effect is not as large as would be expected from compaction ($\varepsilon = 0$).

[31] In unfractured hydrate-bearing sands, an advantage of the TPBE over the effective medium theory (EMT) by *Helgerud et al.* [1999] is that whereas EMT accurately predicts P wave velocities, the S wave velocity is overestimated. TPBE is preferable to the modified Biot-Gassmann theory (BGTL) [*Lee and Collett*, 2005] because TPBE is accurate for all ranges of gas hydrate saturation, including potentially economic methane production targets with gas hydrate saturations above 80%, for which BGTL under-predicts the measured velocity.

Acknowledgments

[32] Schlumberger Ltd. acquired the well logs at the Mallik 5L-38 research well. The well was a collaboration between the Japan National Oil Company, Japan Petroleum Exploration Company, Geological Survey of Canada, U.S. Geological Survey, GeoForschungsZentrum Potsdam, Indian Ministry of Petroleum and Gas, BP-ChevronTexaco-Burlington, U.S. Department of Energy, and the International Continental Scien-

tific Drilling Program. We appreciate the "Mount Elbert" science team for acquiring log data at Mt. Elbert and G. D. Guerin for reprocessing the Tigershark acoustic logs. Continued support from T. S. Collett and discussions with C. Ruppel and J. C. Santamarina are also appreciated.

References

Carcione, J. M., and D. Gei (2004), Gas-hydrate concentration estimated from P- and S-wave velocities at the Mallik 2L-38 research well, Mackenzie Delta, Canada, *J. Appl. Geophys.*, *56*, 73–78, doi:10.1016/j.jappgeo.2004.04.001.

Carcione, J. M., and U. Tinivella (2000), Bottom-simulating reflectors: Seismic velocities and AVO effects, *Geophysics*, *65*, 54–67, doi:10.1190/1.1444725.

Ecker, C., J. Dvorkin, and A. Nur (1998), Sediments with gas hydrates: Internal structure from seismic AVO, *Geophysics*, *63*, 1659–1669, doi:10.1190/1.1444462.

Expedition 311 Scientists (2006), Site U1327, in *Proceedings of the Integrated Ocean Drilling Program*, vol. 311, edited by M. Riedel et al., Integrated Ocean Drill. Program Manage. Int., Inc., Washington, D. C., doi:10.2204/iodp.proc.311.105.2006.

Gassmann, F. (1951), Uber die elastizitat poroser medien, *Vierteljahrsschr. Naturforsch. Ges. Zürich*, *96*, 1–23.

Guerin, G., D. Goldberg, and A. Meltser (1999), Characterization of in situ elastic properties of gas hydrate-bearing sediments on the Blake Ridge, *J. Geophys. Res.*, *104*, 17,781–17,795, doi:10.1029/1999JB900127.

Helgerud, M. B., J. Dvorkin, A. Nur, A. Sakai, and T. Collett (1999), Elastic-wave velocity in marine sediments with gas hydrates: Effective medium modeling, *Geophys. Res. Lett.*, *26*, 2021–2024, doi:10.1029/1999GL900421.

Jakobsen, M., J. A. Hudson, T. A. Minshull, and S. C. Singh (2000), Elastic properties of hydrate-bearing sediment using effective medium theory, *J. Geophys. Res.*, *105*, 561–577, doi:10.1029/1999JB900190.

Kleinberg, R. L., C. Flaum, and T. S. Collett (2005), Magnetic resonance log of JAPEX/JNOC/GSC et al. Mallik 5L-38 gas hydrate production research well: Gas hydrate saturation, growth habit, relative permeability, in *Scientific Results From the Mallik 2002 Gas Hydrate Production Research Well Program, Makenzie Delta, Northwest Territories, Canada*, edited by S. R. Dallimore and T. S. Collett, *Bull. Geol. Surv. Can.*, *585*, 10 pp.

Kuster, G. T., and M. N. Toksöz (1974), Velocity and attenuation of seismic waves in two-phase media: Part 1, Theoretical formulations, *Geophysics*, *39*, 587–606, doi:10.1190/1.1440450.

Kvenvolden, K. A., and T. D. Lorenson (2001), The global occurrence of natural gas hydrates, in *Natural Gas Hydrates: Occurrence, Distribution and Detection*, *Geophys. Monogr. Ser.*, vol. 124, edited by C. K. Paull and W. P. Dillon, pp. 3–18, AGU, Washington, D. C.

Leclaire, P., F. Cohen-Tenoudji, and J. Aguirre-Puente (1994), Extension of Biot's theory of wave propagation to frozen porous media, *J. Acoust. Soc. Am.*, *96*, 3753–3768, doi:10.1121/1.411336.

Lee, M. W. (2005), Proposed moduli of dry rock and their application to predicting elastic velocities of sandstones, *U.S. Geol. Surv. Sci. Invest. Rep.*, *2005-5119*, 14 pp. (Available at http://pubs.usgs.gov/sir/2005/5119/)

Lee, M. W. (2007), Velocities and attenuations of gas hydrate-bearing sediments, *U.S. Geol. Surv. Sci. Invest. Rep.*, *2007-5264*, 11 pp.

Lee, M. W., and T. Collett (1999), Amount of gas hydrate estimated from compressional- and shear-wave velocities at the JPEX/JNOC/GSC Mallik 2L-38 gas hydrate research well, *Bull. Geol. Surv. Can.*, *544*, 313–322.

Lee, M. W., and T. S. Collett (2005), Assessments of gas hydrate concentrations estimated from sonic logs in the JAPEX/JNOC/GSC et al. Mallik 5L-38 gas hydrate research production well, in *Scientific Results From the Mallik 2002 Gas Hydrate Production Research Well Program, Makenzie Delta, Northwest Territories, Canada*, edited by S. R. Dallimore and T. S. Collett, *Bull. Geol. Surv. Can.*, *585*, 10 pp.

Mavko, G., T. Mukerji, and J. Dvorkin (1998), *The Rock Physics Handbook: Tools for Seismic Analysis in Porous Media*, 329 pp., Cambridge Univ. Press, Cambridge, U. K.

Mount Elbert Science Team (2007), Alaska North Slope well successfully cores, logs, and tests gas-hydrate-bearing reservoirs, Fire in the Ice newsletter, winter, pp. 1–4, Natl. Energy Technol. Lab., Off. of Fossil Energy, Dept. of Energy, Washington, D. C.

Pride, S. R., J. G. Berryman, and J. M. Harris (2004), Seismic attenuation due to wave-induced flow, *J. Geophys. Res.*, *109*, B01201, doi:10.1029/2003JB002639.

Sloan, E. D., Jr. (1998), *Clathrate Hydrates of Natural Gases*, 2nd ed., 705 pp., Marcel Dekker, New York.

Smith, S., R. Boswell, T. Collett, M. Lee, and E. Jones (2006), Alaminos Canyon Block 818: A documented example of gas hydrate saturated sand in the Gulf of Mexico, Fire in the Ice newsletter, fall, pp. 12–13, Natl. Energy Technol. Lab., Off. of Fossil Energy, Dept. of Energy, Washington, D. C.

Stoll, R. D., and G. M. Bryan (1979), Physical properties of sediments containing gas hydrates, *J. Geophys. Res.*, *84*, 1629–1634, doi:10.1029/JB084iB04p01629.

Wood, W. T., P. L. Stoffa, and T. H. Shipley (1994), Quantitative detection of methane hydrate through high-resolution seismic velocity analysis, *J. Geophys. Res.*, *99*(B5), 9681–9695, doi:10.1029/94JB00238.